W.Sanz, A.Gehrer, J.Woisetschläger, M.Forstner, W.Artner, H.Jericha (1998) *Numerical and Experimental Investigation of the Wake Flow Downstream of a Linear Turbine Cascade*, Proc. ASME International Gas Turbine and Aeroengine Congress, Stockholm, Sweden, 98-GT-246

NUMERICAL AND EXPERIMENTAL INVESTIGATION OF THE WAKE FLOW DOWNSTREAM OF A LINEAR TURBINE CASCADE

Wolfgang Sanz, Arno Gehrer, Jakob Woisetschläger,
Martin Forstner, Wolfgang Artner and Herbert Jericha
Institute of Thermal Turbomachinery and Machine Dynamics
Graz University of Technology
Graz, Austria

ABSTRACT

In turbomachinery the wake flow together with the inherent unsteadiness caused by interaction between stator and rotor has a significant impact on efficiency and performance. The prediction of the wake flow depends largely on the turbulence modeling. Therefore in this study the evolution of a viscous wake downstream of a linear turbine cascade is experimentally and computationally investigated. In a transonic cascade test stand Laser Doppler Velocimeter (LDV) measurements of velocity and turbulent kinetic energy are done in several axial planes downstream of the blade trailing edge. Two different turbulence models are then incorporated into a two-dimensional Navier-Stokes solver to calculate the turbulent wake flow and the results are compared with the experimental data to test the quality of the turbulence models. The large discrepancies between measurement and calculation are assumed to be caused by the periodic vortex shedding from the blunt trailing edge which is not taken into account by the turbulence models. But further research is needed to resolve this issue.

NOMENCLATURE

a_0	stagnation speed of sound
c	chord length
c_{ax}	axial chord length
e	total energy per unit volume
k	turbulent kinetic energy
l_m	turbulent mixing length
p	pressure
P_k	production of turbulent kinetic energy
PS	pressure side
S	surface of a computational cell
s	spacing
SS	suction side
t	time
Tu	turbulence intensity
u_i	cartesian velocity components
u_i'	velocity fluctuations
V	area of a computational cell
W_{in}	inlet velocity
x_i	cartesian coordinates
y	minimum distance to the wall
δ	shear layer thickness
δ_{ij}	Kronecker delta
ε	dissipation of turbulent kinetic energy
μ, μ_t	molecular and turbulent viscosity
ρ	density
Ω	flow vorticity
$\vec{n}$	surface normal unitvector
$\vec{w}$	velocity vector
$\vec{\tau}^S$	surface shear stress vector
$\tau_{ij}{}_S$	components of the shear stress tensor
$\dot{q}^S$	surface heat flux
q_i	surface heat flux vector
E, $\mathbf{E}^{SA}$, $\mathbf{E}^{k\varepsilon}$	convective fluxes
Q, $\mathbf{Q}^{k\varepsilon}$	vector of conservative variables
R, $\mathbf{R}^{SA}$, $\mathbf{R}^{k\varepsilon}$	diffusive fluxes

INTRODUCTION

In turbomachinery the wake flow together with the inherent unsteadiness caused by interaction between stator and rotor has a significant impact on efficiency and performance. Wakes generated by a blade row travel downstream and interact with the succeeding blade

rows affecting pressure distribution, heat transfer and boundary layer development. Numerical predictions to study the influence of wakes on aerodynamic losses and heat transfer need correct inlet boundary conditions for single row calculations and a correct modeling of wake propagation and decay in the axial gap for single and multi stage calculations. Therefore an increasing amount of research work has been focused on wake development and its evolution in the axial gap as well as within the blade row.

Schobeiri et al. (1996) studied the development of two-dimensional wakes within curved channels and established a theoretical framework. Ames and Plesniak (1997) investigated the influence of combustor-like inlet turbulence on turbine vane wake characteristics, development and mixing. For four different inlet turbulence levels flow quantities and turbulence characteristics were carefully measured at three positions downstream of a vane cascade and the data analyzed to determine the wake evolution. Adamczyk et al. (1996) conducted a numerical study to investigate the wake rectification process and showed that there is a major difference between an isolated rotor and a rotor operating in a multiple-blade-row environment. Stauter et al. (1991) studied the temporal and spatial variations in the midspan aerodynamics of the second stage of a two-stage compressor and reported data of rotor and stator wake structure and decay. This flow was computationally investigated by Gundy-Burlet et al. (1991) using an unsteady thin-layer two-dimensional Navier-Stokes solver with an algebraic Baldwin-Lomax turbulence model. Generally, the agreement was good between the measured and computed time-averaged result compared at one axial position downstream of the rotor for wake depth, width and tangential location. The agreement between the measured and computed fluctuations was also reasonably good. A similar computational investigation was done by Ho and Lakshminarayana (1995) who used a two-dimensional low-Re k-ε turbulence model. Upstream of the stator blade the predicted and measured tangential velocity profiles agreed well, whereas the predicted deficit in the axial velocity profile decayed much faster. Downstream of the stator the time mean profiles were predicted well, whereas there was little agreement in the velocity fluctuations.

Luo and Lakshminarayana (1997) calculated the flow field through the nozzle passage of a single-stage turbine and compared the wake flow close to the trailing edge with the measurements of Zaccaria and Lakshminarayana (1995). They used a three-dimenensional Navier-Stokes solver with a low-Re k-ε model and a zonal k-ε/algebraic Reynolds-stress model. The predictions from both turbulence models are quite close for all downstream locations. The discrepancy between the prediction and the data is largest at the midspan region. One reason is that the k-ε model predicted an earlier transition on the suction side and hence a thicker boundary layer leading to an overprediction of the wake width. Other reasons could also be the influence of the downstream rotor and the error in measuring caused by using a five-hole probe in the wake. In 1997 Zaccaria and Lakshminarayana presented detailed measurements of the rotor wake profiles of the same turbine at a large number of locations and developed correlations for the decay characteristics.

As e.g. Luo and Lakshminarayana (1997) showed the prediction of the wake flow depends largely on the turbulence modeling, because it influences blade boundary layers and wake mixing mechanism. Although many interesting works about wake flow are published as shown above only few researchers compared the performance of different turbulence models and studied the wake evolution at several locations. Therefore in this study the evolution of a viscous wake downstream of a linear turbine cascade is experimentally and computationally investigated. The flow field is two dimensional so that no three-dimensional effects influence the wake flow evolution. In a transonic cascade test stand LDV measurements of velocity and turbulent kinetic energy are done in several axial planes downstream of the blade trailing edge. Two different turbulence models are then incorporated into a two-dimensional Navier-Stokes solver to calculate the turbulent wake flow and the results are compared with the experimental data to test the quality of the turbulence models.

EXPERIMENTAL FACILITY

The experiment was carried out in a linear cascade wind tunnel capable of supersonic inlet flow. Air is supplied by a compressor station consisting of two turbo compressors and one screw compressor with a total electric power of 2.8 MW. The turbine cascade consists of 7 blades as described by Kiock et al. (1986) (see Fig. 1). The major blade geometries are summarized in table 1. To monitor the uniformity of the inlet flow, seven static pressure taps are arranged across two passages at the inlet; two rows of static pressure taps are arranged at the exit. The three middle blades are also equipped with static pressure taps to control the periodicity of the flow, which can be set by a tailboard. Total pressure and total temperature are measured at inlet and exit by probes. The location of all pressure taps is shown in Fig. 1. Glass windows of 15mm thickness are built in the side walls to allow optical access to the mid flow passage and to the inlet and exit region. The flow conditions in the experiment are subsonic as shown in table 1. The inlet turbulent kinetic energy k of 5.9 m^2/s^2 corresponds to a turbulence intensity Tu of 2.5 %.

The wake flow downstream of the trailing edge is measured with a Laser-Doppler Velocimeter (LDV). The LDV is a two-dimensional measuring system with a 6 W argon ion laser. The seeding material is DEHS oil with a particle size of about 0.5 μm. The measurement data in the wake are acquired at midspan at three axial planes located downstream of the cascade at x/c_{ax} = 0.037, 0.161 and 0.285 as shown in Fig. 2. The first plane is located in the trailing edge region of the wake, where the velocity defect is very large. The other planes are in the near wake region, where the wake defect is still in the order of the mean velocity and where blade geometry and loading are mainly influencing the wake. This classification is made according to Zaccaria and Lakshminarayana (1997). The distance of the third plane corresponds to the rotor-stator spacing of modern axial flow turbines.

According to the number of validated measuring signals an error analysis is done based on the assumption of a Gaussian distribution of the velocity. The uncertainty for a 95 percent confidence level is for the mean velocity 5 percent inside and 0.2 percent outside the wake in the first measuring plane and 1.8 and 0.2 percent, respectively, for the other two planes. The uncertainty of the turbulence level as the standard deviation of the velocity is due to the nature of this error analysis much higher, especially in the trailing edge region where only few valid data samples are counted. It is 60 percent inside and 22 percent outside the wake in the first measuring plane and 22 and 22 percent, respectively, for the other two planes.

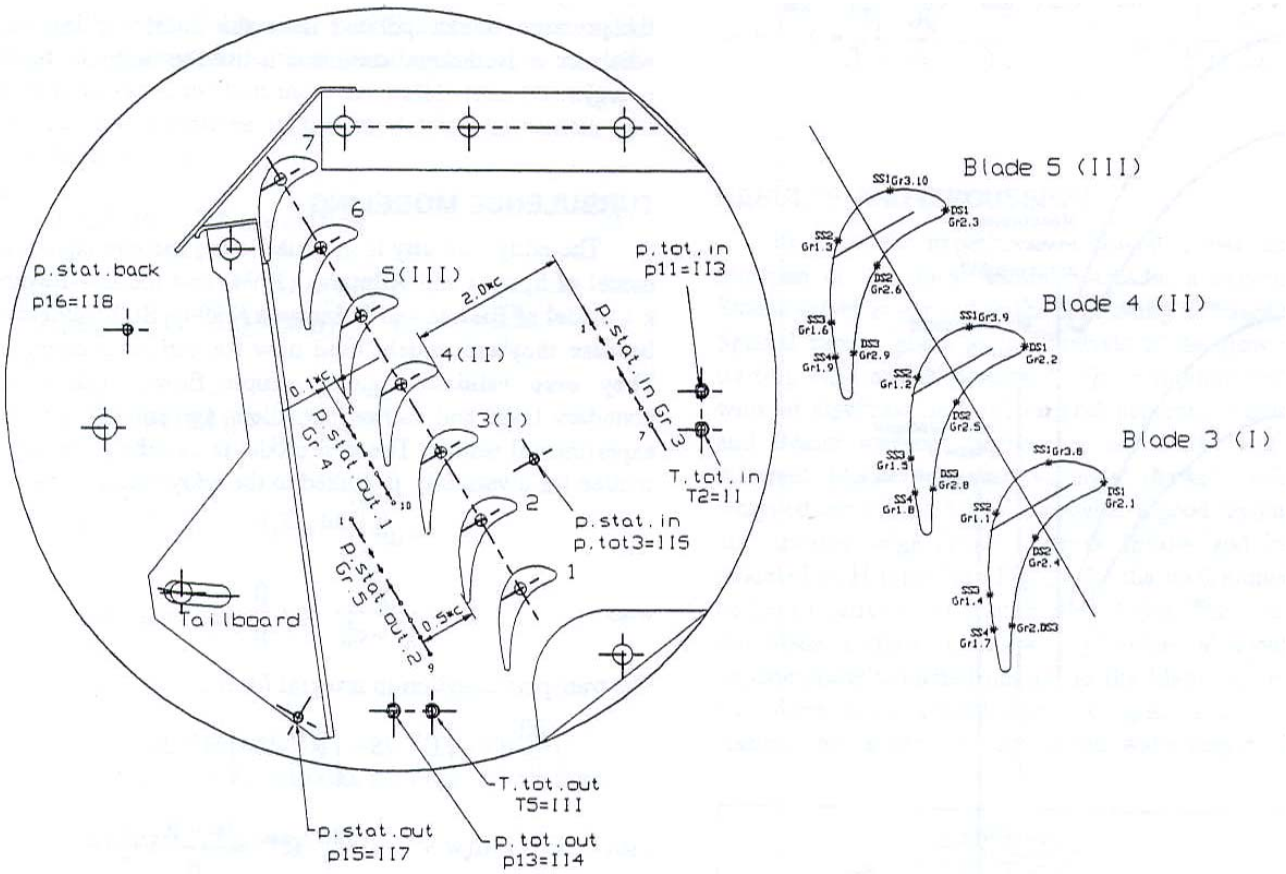

Fig. 1: Schematic of linear cascade and pressure tap location

Table 1: Blade geometry and flow conditions

Blade number	7
Chord length	58 mm
Axial chord length	48.4 mm
Spacing	41.18 mm
Span	100 mm
Stagger angle	30°
Inlet total pressure	1.3 bar
Inlet total temperature	311.1 K
Isentropic exit Mach number	0.624
Exit Reynolds number	842000
Inlet turbulence intensity	2.5 %

NUMERICAL APPROACH

The compressible, Reynolds-averaged continuity-, momentum- and energy equation in integral form are used to model the fluid flow:

$$\int_V \frac{\partial \mathbf{Q}}{\partial t} dV + \int_S \mathbf{E} dS - \int_S \mathbf{R} dS = 0 \qquad (1)$$

with

$$\mathbf{Q} = [\rho, \rho\vec{w}, e]^T; \mathbf{E} = [\rho(\vec{w}\cdot\vec{n}), \rho\vec{w}(\vec{w}\cdot\vec{n}) + p\vec{n}, (e+p)(\vec{w}\cdot\vec{n})]^T;$$
$$\mathbf{R} = [0, \vec{\tau}^S, \vec{\tau}^S\cdot\vec{w} + \dot{q}^S]^T$$
$$\vec{\tau}^S = \begin{bmatrix} \tau_{xx} & \tau_{xy} \\ \tau_{xy} & \tau_{yy} \end{bmatrix} \cdot \vec{n}; \quad \dot{q}^S = \begin{bmatrix} \dot{q}_x \\ \dot{q}_y \end{bmatrix} \cdot \vec{n}$$

The pressure is related to the other flow quantities through the equation of state for a perfect gas. The shear stresses, τ_{ij} , are divided into a laminar and a turbulent part. The laminar parts, τ_{ij}^{lam} , are given directly by Eq.(2).

$$\tau_{ij}^{lam} = \mu\left(\frac{\partial u_i}{\partial x_j} + \frac{\partial u_j}{\partial x_i} - \frac{2}{3}\frac{\partial u_k}{\partial x_k}\delta_{ij}\right) \qquad (2)$$

The turbulent stresses are calculated using the Boussinesq assumption, which relates the turbulent stress tensor with the mean strain-rate tensor by an eddy viscosity μ_t. The eddy viscosity is calculated using an appropriate turbulence model (see below).

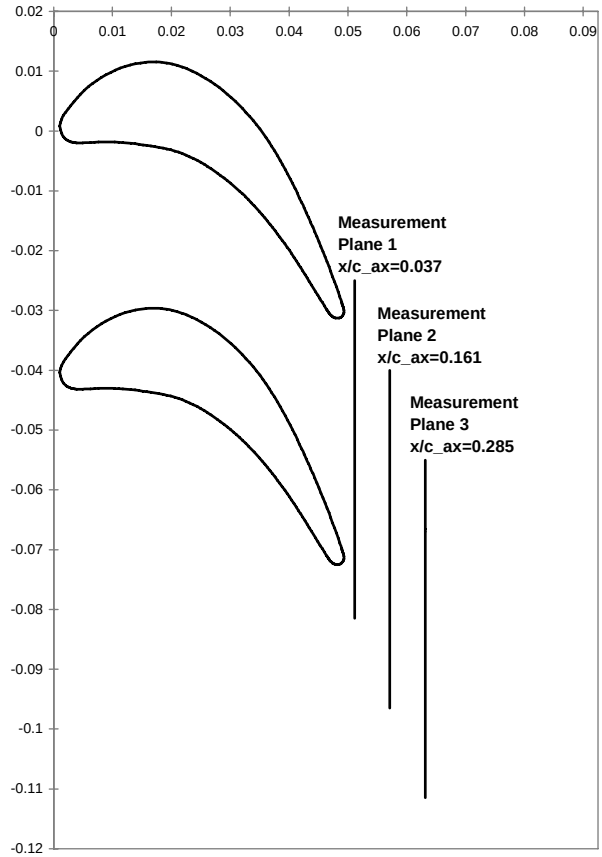

Fig. 2: Measurement planes in the wake flow field

$$\tau_{ij}^{turb} = -\overline{\rho u_i' u_j'} = \mu_t\left(\frac{\partial u_i}{\partial x_j}+\frac{\partial u_j}{\partial x_i}-\frac{2}{3}\frac{\partial u_k}{\partial x_k}\delta_{ij}\right)-\frac{2}{3}\rho k\delta_{ij} \qquad (3)$$

The heat-flux, q_i , is treated in a similar way according to Reynolds analogy. For these calculations a constant turbulent Prandtl number of Pr_t=0.9 is assumed.

The governing equations (Eq. (1)) are treated in conservative form and discretized in time using the Euler implicit method leading to a set of non-linear finite difference equations which is solved using a Newton procedure. A local time-step is applied to enhance convergence. The convective (Euler) fluxes are discretized using a third-order-accurate, TVD-upwind, cell-centered finite-volume scheme. In contrast to this the transport equations for the turbulent quantities are solved using a more stable first-order upwind scheme, after a comparison between results using first-order and third-order accurate discretization showed only a negligible difference in the wake flow field. The TVD scheme is based on Roe's approximate Riemann solver (Roe, 1981). The viscous fluxes are evaluated by central-differencing applying Green's theorem. The time linearization of the viscous flux vector is performed by applying the thin-layer approximation to the implicit side of the equations (Gehrer and Jericha, 1997).

Phantom cells are used to handle all boundaries. Flow angle, total pressure and total temperature are prescribed at the inflow boundary and static pressure at the outflow boundary. On solid walls, the pressure is extrapolated from the interior points and a no-slip adiabatic or isothermal condition is used to compute density and total energy.

TURBULENCE MODELING

The eddy viscosity is modeled using the one-equation turbulence model of Spalart and Allmaras (1994) and the low-Reynolds-number k-ε model of Biswas and Fukuyama (1994). Both models were chosen because they are widely used now for turbomachinery calculations. They were validated against simple flows, such as a flat plate boundary layer and showed excellent agreement with the published experimental results. The first model is based on a transport equation written for a variable $\tilde{\mu}$ linked to the eddy viscosity by

$$\mu_t = f_{v1}\tilde{\mu} \qquad (4)$$

with $$f_{v1} = \frac{\chi^3}{\chi^3 + c_{v1}^3} \quad \chi = \frac{\tilde{\mu}}{\mu}$$

The transport equation in integral form is:

$$\int_V \frac{\partial \tilde{\mu}}{\partial t} dV + \int_S \mathbf{E}^{SA}\, dS - \int_S \mathbf{R}^{SA}\, dS = \int_V \mathbf{H}^{SA}\, dV \qquad (5)$$

with $$\mathbf{E}^{SA} = \tilde{\mu}(\vec{w}\cdot\vec{n}) \qquad \mathbf{R}^{SA} = \frac{\mu+\tilde{\mu}}{\sigma}\nabla\left(\frac{\tilde{\mu}}{\rho}\right)\cdot\vec{n}$$

This equation is similar to the governing flow equations (Eq. (1)), except for the source term $\mathbf{H}^{SA}$, which consists of a turbulence production and destruction term, a diffusion term and an ignition term to model laminar to turbulent transition.

$$\mathbf{H}^{SA} = c_{b1}(1-f_{t2})\tilde{S}\tilde{\mu} - \left(\frac{c_{w1}f_w}{\rho} - \frac{c_{b1}}{\rho\kappa^2}f_{t2}\right)\left(\frac{\tilde{\mu}}{y}\right)^2 + \frac{\rho c_{b2}}{\sigma}\left(\nabla\left(\frac{\tilde{\mu}}{\rho}\right)\right)^2 + \rho f_{t1}(\Delta V)^2 \qquad (6)$$

In this investigation fully turbulent flow is assumed, so that f_{t1} and f_{t2} are set to zero. The other model quantities are defined as follows.

$$\tilde{S} = |\Omega| + \frac{\tilde{\mu}}{\rho\kappa^2 y^2}f_{v2} \qquad f_{v2} = 1 - \frac{\chi}{1+c_{v1}f_{v1}} \qquad f_w = g\left(\frac{1+C_{w3}^6}{g^6+C_{w3}^6}\right)^{\frac{1}{6}}$$

$$g = r + c_{w2}(r^6 - r) \qquad r = \frac{\tilde{\mu}}{\rho\tilde{S}\kappa^2 y^2} \qquad (7)$$

$$c_{b1} = 0.1355; c_{b2} = 0.622; c_{w1} = \frac{c_{b1}}{\kappa^2} + \frac{1+c_{b2}}{\sigma};\ c_{w2} = 0.3; c_{w3} = 2.0;$$

$$c_{v1} = 7.1; \sigma = \frac{2}{3}; \kappa = 0.41; c_{t1} = 1; c_{t2} = 2; c_{t3} = 1.2; c_{t4} = 0.5$$

This equation was derived for flows in free air and therefore it cannot consider higher free-stream turbulence levels. So the inflow value was set to $\tilde{\mu}/\mu = 0.1$, according to Spalart and Allmaras (1994), which implies a very small eddy viscosity. At solid walls $\tilde{\mu}$ is set to zero, at the outlet boundary a simple extrapolation is used.

The second model is a low-Reynolds-number k-ε model developed by Biswas and Fukuyama (1994), which uses field equations to describe characteristic turbulence scales. It is chosen because it is said to model transition more accurately than other low-Re k-ε models. The two equations of this model can be written in integral form similar to Eq.(5):

$$\int_V \frac{\partial \mathbf{Q}^{k\varepsilon}}{\partial t} dV + \int_S \mathbf{E}^{k\varepsilon} dS - \int_S \mathbf{R}^{k\varepsilon} dS = \int_V \mathbf{H}^{k\varepsilon} dV \qquad (8)$$

with $\mathbf{Q}^{k\varepsilon} = [\rho k, \rho\varepsilon]^T$ $\mathbf{E}^{k\varepsilon} = \mathbf{Q}^{k\varepsilon}(\vec{w}\cdot\vec{n})$ $P_k = \tau_{ij}^{turb} \frac{\partial u_i}{\partial x_j}$

$$\mathbf{R}^{k\varepsilon} = \left[\left(\mu + \frac{\mu_t}{Pr_k}\right)\nabla k \cdot \vec{n}, \left(\mu + \frac{\mu_t}{Pr_\varepsilon}\right)\nabla \varepsilon \cdot \vec{n} \right]^T$$

$$\mathbf{H}^{k\varepsilon} = \left[P_k - \rho\varepsilon, \frac{\varepsilon}{k}\left(f_1 C_{\varepsilon_1} P_k - f_2 C_{\varepsilon_2} \rho\varepsilon\right) \right]^T$$

The eddy viscosity is obtained from

$$\mu_t = C_\mu f_\mu \frac{\rho k^2}{\varepsilon} \qquad (9)$$

The damping functions and model constants are defined as follows:

$$f_\mu = [1 - EXP(-Re_t/150)][1 + 18.5/Re_t]$$
$$f_1 = 1 + 0.3EXP\left(-(Re_t/50)^2\right)$$
$$f_2 = \left[1 - 0.3EXP\left(-(Re_t/6.5)^2\right)\right][1 - EXP(-Re_y/10)]$$
$$Re_y = \frac{\rho y\sqrt{k}}{\mu} \qquad Re_t = \frac{\rho k^2}{\mu\varepsilon}$$
$$C_\mu = 0.09; C_{\varepsilon_1} = 1.46; C_{\varepsilon_2} = 1.9; Pr_k = 1.4; Pr_\varepsilon = 1.3 \qquad (10)$$

The boundary conditions are k=0, $\partial\varepsilon/\partial y = 0$ at solid walls and $k = 3Tu^2 W_{in}^2/2$, $\varepsilon = C_\mu^{3/4} k^{3/2}/l_m$ at the inlet, a simple extrapolation is used at the outlet boundary. Whereas the turbulence intensity Tu is mostly known from measurements, it is difficult to estimate the turbulent mixing length l_m. In turbomachinery applications l_m is usually set to a value between 1% and 10% of a characteristic length scale. To study the sensitivity of the solution to the prescribed value calculations are done for an inlet mixing length of 1% and 10% of the spacing.

Most k-ε models produce too much turbulent energy in stagnation point regions. This is because the Boussinesq assumption fails in flows with large normal strain which results in excessive production of turbulent energy in stagnation flows. These disturbances are convected downstream and can influence the entire boundary layer. One way to overcome this problem is using a modified production term. In our calculations the modification of Kato and Launder (1993) is used which replaces the strain rate by the vorticity in the production according to following formulation:

$$P_k = \mu_t \cdot S \cdot \Omega \qquad (11)$$

with $S = \sqrt{\frac{1}{2}\left(\frac{\partial u_i}{\partial x_j} + \frac{\partial u_j}{\partial x_i}\right)^2}$ $\Omega = \sqrt{\frac{1}{2}\left(\frac{\partial u_i}{\partial x_j} - \frac{\partial u_j}{\partial x_i}\right)^2}$ (11)

RESULTS AND DISCUSSION

Because the experiments showed a two-dimensional flow at midspan of the linear turbine cascade, a two-dimensional Navier-Stokes solver is applied to the flow using different turbulence models. Special care is given to the analysis of the flow downstream of the trailing edge and in the wake. The computational grid is generated with an algebraic multi-block grid generator based on Bézier curves and Bézier surfaces (Gehrer et al., 1996) and consists of three different blocks to avoid strongly skewed cells. An O-mesh is wrapped around the blade to provide a good resolution of the leading and trailing edge flow, whereas inflow and outflow region are modeled by H-grids (see Fig. 3). So the total number of grid cells can be kept relatively small with about 8500. The size of the first cell at the blade surface is below a y^+-value of about 0.4, the grid is exponentially stretched normal to the blade. A grid sensitivity study was done using a very fine C-O grid of about 23000 cells. The comparison of the velocity in the wake region showed only small differences in the wake flow close to the

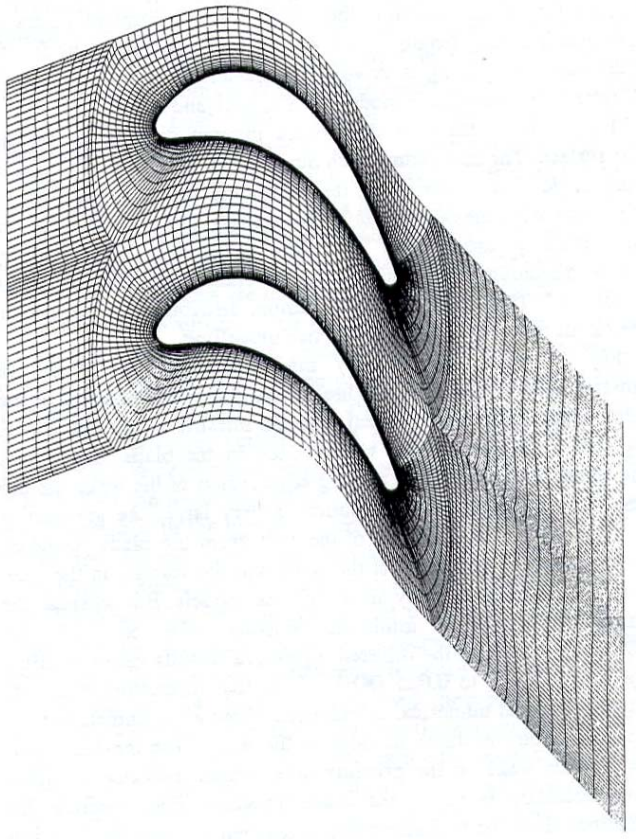

Fig. 3: Computational grid for linear turbine cascade

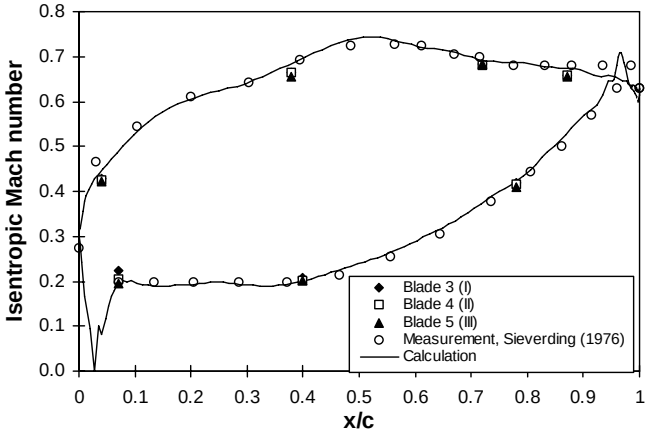

Fig. 4: Comparison of measured and calculated isentropic Mach number distribution, M = 0.624, Re=842000

trailing edge. The turbulence level was predicted smaller for the fine grid, but the difference was small in comparison to the differences to the measurement data.

The one-equation Spalart-Allmaras turbulence model and the Kato-Launder modification of the two-equation low-Re k-ε model are used. Due to the uncertainty in prescribing an inlet boundary condition for the dissipation ε, the results for two different values of the turbulent mixing length l_m, 1% and 10% of a characteristic length (in this case the spacing is chosen) are presented. In this chapter we will refer to the turbulence models as SA, KE1 and KE10.

Fig. 4 shows the isentropic Mach number distribution on the blade surface. The maximum Mach number is 0.75 at the suction side of the blade. The accuracy of the numerical result is verified by comparison with measurements of Sieverding (1976) and with the own surface pressure data. The flow periodicity controlled by pressure measurements at three adjacent blades (see also Fig. 1) is also fulfilled. This predicted Mach number distribution is largely the same for all three variants of turbulence modelling.

Fig. 5 shows the velocity made dimensionless with the stagnation speed of sound a_0 in three axial planes downstream of the trailing edge. Some measurement data are missing in the first plane, since one of the laser beams was blocked by the blade. In the first plane which is located in the trailing edge region of the wake the dip in the tangential velocity distribution is very large, the gradient is very high due to the transition of the flow from the blade boundary layer to the wake. The width of the wake and the velocity in the free-stream are predicted well by all turbulence models. But whereas the measurements show a minimum velocity w/a_0 of 0.24, the corresponding value of the different numerical results varies within a range of 0.15 (SA) to 0.025 (KE1). It is also interesting that both measurements and numerical calculations show an asymmetry of the wake profile, but on different sides of the wake. The measurements show a wider wake on the pressure side, which indicates a thicker surface boundary layer on the blade pressure side, whereas the calculations show the opposite which seems more reasonable and was also observed by Zaccaria and Lakshminarayana (1997) in their rotor wake measurements. A reason for this discrepancy could be flow separation on the pressure side near

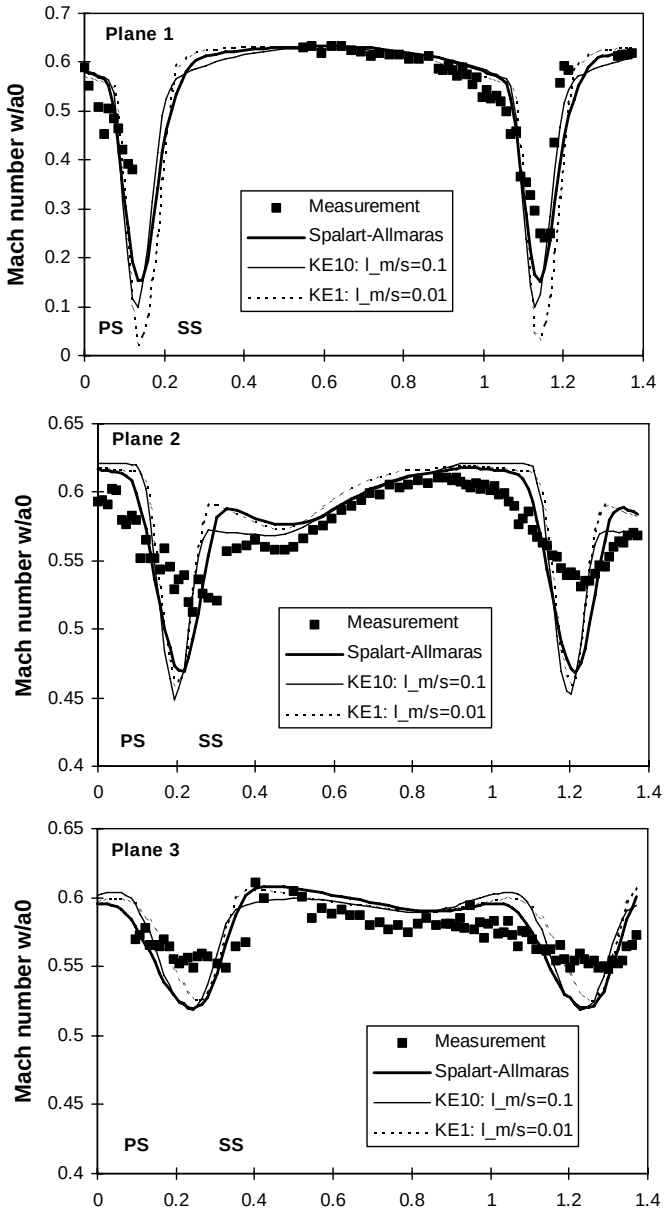

Fig. 5: Velocity distribution in the wake flow field

the trailing edge. A closer investigation of the boundary layer flow there is needed.

Further downstream, in the near wake region, the velocity defect decays and the wake spreads due to mixing and exchange of momentum and energy with the free-stream flow. The numerical results predict this trend, but they show a much slower decay of the wake than the measurements. The measured wake widens more and the velocity defect (defined as the difference of maximum and minimum velocity in the plane made dimensionless by the maximum velocity) in the third plane, at a streamwise distance of about 75% of the axial chord length, reduces to about 10 %, whereas the calculations still predict a velocity defect of about 14 %. The numerical results agree quite well with each other, especially in the free-stream flow.

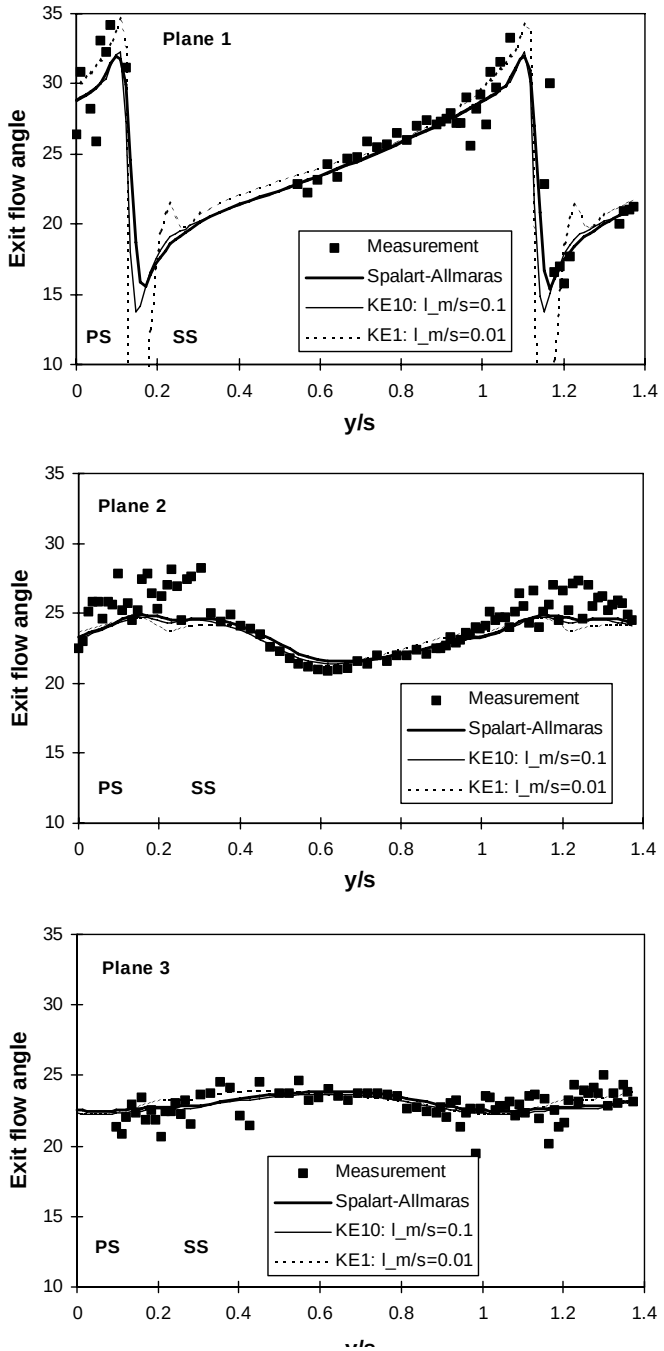

Fig. 6: Exit flow angle in the wake flow field

numerical results agree quite well with each other, especially in the free-stream flow. For the k-ε model KE1 the shorter mixing length, and therefore higher dissipation, at the inlet leads to a higher velocity defect close to the trailing edge, but it also accelerates the spreading of the wake compared to KE10 and SA. It is interesting that in the second plane a small dip in the velocity distribution is measured close to the suction side of the wake which is also predicted by all turbulence

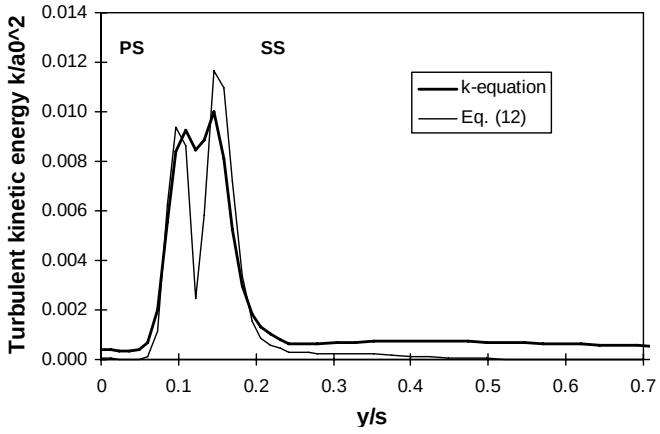

Fig. 7: Comparison of turbulent kinetic energy predicted by k-equation and Eq. (12) for KE1, plane 1

models. This dip is transported in tangential direction as can be seen in the mid of the third measuring plane.

Luo and Lakshminarayana (1997) observed a similar discrepancy between predictions and experimental data at midspan of the nozzle wake. Very close to the trailing edge (x/c_{ax}=0.009) there is excellent agreement, whereas at x/c_{ax}=0.025 and 0.09 the wake depth, but also the wake width is overpredicted. They explain the difference with an overprediction of the boundary layer thickness due to a too early transition on the suction side. In contrast to their experience in this work a fully turbulent flow (SA) as well as a mainly laminar flow (KE1, see below) both result in similar wake defects. A more detailed look at the flow field close to the trailing edge shows two steady counterrotating vortices, whereas in the experiment periodic vortex shedding is observed at the blunt trailing edge. It is possible that the downstream moving vortices cause a faster spreading of the wake.

Fig. 6 shows the measured and calculated exit flow angles. Close to the trailing edge there is a large deviation from the design angle of 22.2°. The calculations are in close agreement with the measurements and predict the overturning on the suction side and underturning on the pressure side due to the blade contour. Only KE1 shows larger deviations, especially close to the center of the wake, where negative flow angles are predicted. This can also be explained by the existence of the counterrotating vortices. KE1 predicts a length of the vortex region of 8.5 % axial chord length in comparison to SA with 5.6%, so that for KE1 the measuring plane is still located in the vortex region. It also agrees with the higher velocity defect of KE1 observed in Fig. 5. In the second plane the deviation of the flow angle has considerably decreased, the calculations show a smaller flow angle than the measuring data, which are yet too largely scattered. In the third plane the agreement between measurement and calculations is good. Again there is a slight difference between KE1 and KE10/SA.

To explain the differences between measured and calculated wake characteristics, the turbulent kinetic energy in the wake is investigated. Because SA does not explicitly predict the turbulent kinetic energy, the following equation which was derived from the Prandtl mixing length formulation and the eddy viscosity definition of the k-ε equation (Eq. (9)) is used:

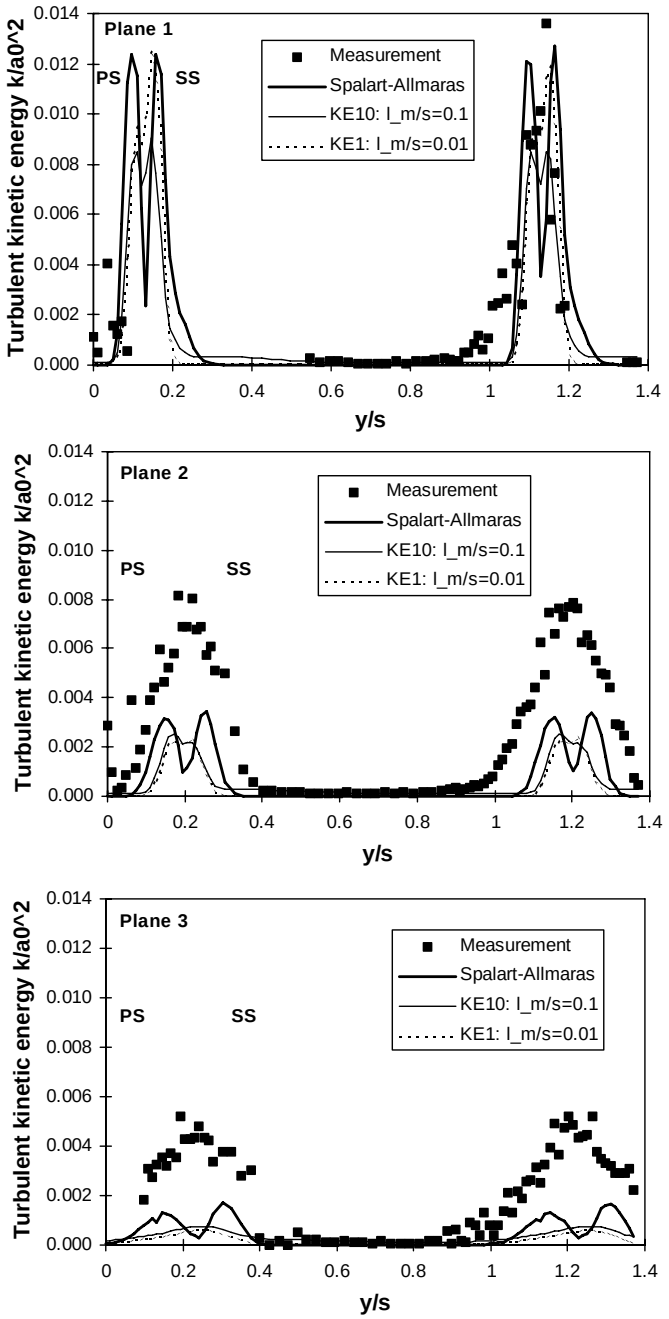

Fig. 8: Turbulent kinetic energy distribution in the wake flow field

$$k = \mu_t \frac{\Omega}{\rho\sqrt{C_\mu}} \tag{12}$$

To verify the validity of this formulation the turbulent kinetic energy predicted by KE1 is compared with Eq. (12) in Fig. 7. We see that there is relatively good agreement at the sides of the wake, but poor agreement in the wake center and in the free-stream. This is reasonable because Prandtl's formulation is only valid for the inner part of a turbulent boundary layer, where the high shear stresses are similar to the ones at the sides of the wake. The results of SA in Fig. 8, which shows the turbulent kinetic energy in the wake flow, have to be seen under this limitation. The measurement data of k show a large scatter due to the high uncertainty in the turbulence level determination.

In the trailing edge region measurement and calculations agree qualitatively well, although the large uncertainty does not allow a quantitative comparison inside the wake. The maximum kinetic energy is of the same level, although the measurements show a slightly wider turbulence zone. All the numerical results predict a dip in the wake center and a maximum on either side of the dip. This can be explained by the fact, that the turbulence is zero on the blade surface and has a maximum slightly away from the surface. SA and KE10 show a symmetric turbulence distribution, whereas KE1 predicts a distinct maximum on the suction side of the wake indicating a higher turbulence level in the suction surface boundary layer of the blade. The reason for this is that due to the higher dissipation at the inlet boundary the flow remains laminar till close to the trailing edge where it tends to separate. On the other hand, in the free stream KE10 predicts a slightly higher turbulence level close to the suction side of the wake.

More downstream in the near wake region the turbulent kinetic energy decreases. In the wake region it is strongly underpredicted by all turbulence models, the turbulence level is twice (plane 2) to three-times (plane 3) higher in the measurements. This cannot be explained by the high uncertainty of the LDV data but by the nature of LDV measurements which count not only the random turbulent fluctuations but also the periodic fluctuations of the shedding vortices for the turbulence level. The turbulence models cannot take into account these periodic fluctuations. Further research is needed to resolve this issue. A time-accurate computation may be necessary to capture the wake flow field accurately and a phase-locked ensemble-averaging technique should be applied so separate periodic and random contributions to the instantaneous LDV data as described by Zunino et al. (1997).

SA shows a higher turbulence level than KE10 and KE1, especially in the third plane where it predicts a twice as high turbulent kinetic energy. The predicted turbulence dissipation of SA seems to be much smaller. The dip in the wake center can still be seen in the second plane, whereas it is vanished in the third measuring plane. KE10 predicts a higher turbulence than KE1 due to smaller turbulence dissipation at the inlet boundary.

Although not measured, the computed turbulent shear stress is compared in Fig. 9 because it can be directly determined by all turbulence models. The turbulent shear stress is very small in the free stream and has its maximum inside the wake, because it results from velocity and turbulence gradients. It changes sign near the wake center because of the opposite gradients on either side of the wake. In the first two planes the zero turbulent shear stress is not located at the point of minimum velocity, which was also observed by Zaccaria and Lakshminarayana (1997). They also noticed the asymmetry of the shear stress profiles, but they measured higher values on the pressure side which is in contrast with these numerical results. This difference decreases fast on the way downstream. Again SA predicts a much slower decrease of the turbulent shear stresses than KE10 and KE1. It is interesting that KE10 also predicts a relatively high and oscillating

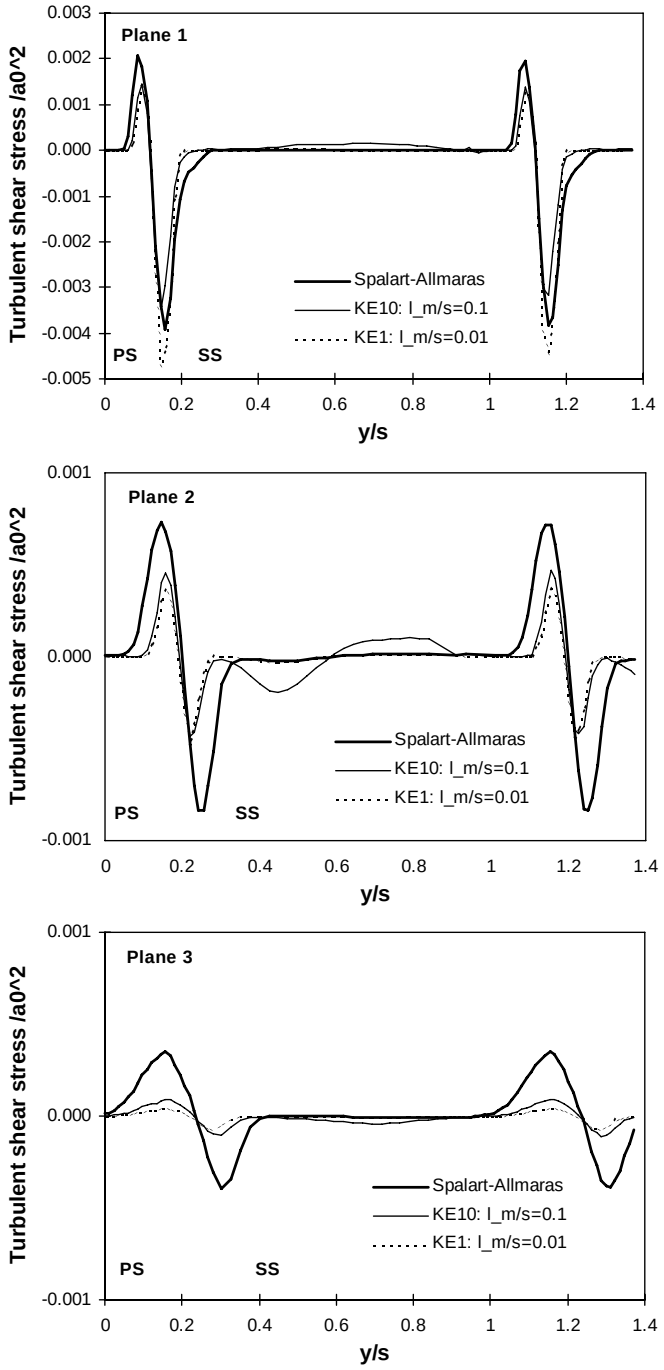

Fig. 9: Turbulent shear stress distribution in the wake flow field

value of the shear stress outside of the wake. The reason for this is found in a broad zone of high vorticity on the suction side of the blade caused by the long turbulent mixing length at the inflow boundary which is transported downstream. This zone is outside of the boundary layer on the blade suction side, so that it does not influence the wake flow which is dominated by the boundary layer shed from the suction and pressure side of the blade.

CONCLUSION

The wake flow field of a linear turbine cascade was measured in a wind tunnel and calculated with a two-dimensional upwind-biased Navier-Stokes solver using two different turbulence models. The wake velocity defect was predicted well in the trailing edge region, but largely overpredicted in the near wake region. The turbulence quantities in the wake also show good qualitative agreement close to the trailing edge, but there is a large difference between computed and measured data in the near wake region. It is assumed that this discrepancy can be explained by the periodic vortex shedding at the blunt trailing edge which is not modelled by the steady calculations. The LDV measurements count both the random and periodic fluctuations whereas the turbulence models cannot consider the periodic fluctuations.

Further research is needed to resolve this issue. A time-accurate computation may be necessary to capture the wake flow field accurately and a phase-locked ensemble-averaging technique should be applied so separate periodic and random contributions to the instantaneous LDV data.

All turbulence models show mainly similar behavior. The influence of the value of the turbulent mixing length at the inlet boundary is most evident in the trailing edge region of the wake. A shorter mixing length leads to a remarkably longer zone of counterrotating vortices which can be seen in the flow angles in this region and to a slightly smaller turbulence level in the wake flow field, but in general the influence is small. The Spalart-Allmaras predicts a smaller turbulence dissipation and therefore a much slower decay of the turbulence level in the wake flow field.

ACKNOWLEDGEMENTS

The authors gratefully acknowledge the support of the Austrian Science Foundation (FWF) of this work and of ongoing research in efficiency improvement and emission reduction of thermal power plants.

REFERENCES

Adamczyk, J.J., Celestina, M.L., Chen, J.P., 1996, "Wake-Induced Unsteady Flows: Their Impact on Rotor Performance and Wake Rectification", ASME Journal of Turbomachinery, Vol. 118, pp. 89-95

Ames, F.E., Plesniak, M.W., 1997, "The Influence of Large-Scale, High-Intensity Turbulence on Vane Aerodynamic Losses, Wake Growth, and the Exit Turbulence Parameters", ASME Journal of Turbomachinery, Vol. 119, pp. 182-192

Biswas, D., Fukuyama, Y., 1994, "Calculation of Transitional Boundary Layers With an Improved Low Reynolds Number Version of the k-e Turbulence Model", ASME Journal of Turbomachinery, Vol. 116, pp 765-773

Gehrer A., Paßrucker H., Jericha H., Lang J., 1996, "Blade design and Grid generation for Computational Fluid Dynamics (CFD) with Bézier-curves and Bézier-surfaces", Proceedings of the 2nd European Conference on "Turbomachinery – Fluid Dynamics and Thermodynamics", Antwerpen

Gehrer, A., Jericha, H., 1997, "External Heat Transfer Predictions in a Highly-Loaded Transonic Linear Turbine Guide Vane Cascade Using an Upwind-Biased Navier-Stokes Solver", submitted to ASME Turbo Expo '98

Gundy-Burlet, K.L., Rai, M.M., Stauter, R.C., Dring, R.P., 1991, "Temporally and Spatially Resolved Flow in a Two-Stage Axial Compressor: Par 2 – Computational Assessment", ASME Journal of Turbomachinery, Vol. 113, pp. 227-232

Ho, Y.-H., Lakshminarayana, B., 1995, "Computation of Unsteady Viscous Flow Through Turbomachinery Blade Row Due to Upstream Rotor Wakes", ASME Journal of Turbomachinery, Vol. 117, pp. 541-552

Kato, M., Launder, B.E., 1993 "The modeling of turbulent flow around stationary and vibrating square cylinders", Proc. 9th Symposium on Turbulent Shear Flows, Kyoto, pages 10.4.1-10.4.6, August. 1993

Kiock, R., Lehthaus, F., Baines, N.C., Sieverding, C.H., 1986, "The Transonic Flow Through a Plane Turbine Cascade as Measured in Four European Wind Tunnels", ASME Journal of Engineering for Gas Turbines and Power, Vol. 108, pp. 277-284

Luo, J., Lakshminarayana, B., 1997, "Three-Dimensional Navier-Stokes Computation of Turbine Nozzle Flow With Advanced Turbulence Models", ASME Journal of Turbomachinery, Vol. 119, pp. 516-530

Roe, P.L., 1981, "Approximate Riemann Solvers, Parameter Vectors and Difference Schemes", Journal of Computational Physics, Vol. 43

Schobeiri, M.T., John, J., Pappu, K., 1996, "Development of Two-Dimensional Wakes Within Curved Channels: Theoretical Framework and Experimental Investigation", ASME Journal of Turbomachinery, Vol. 118, pp. 506-518

Sieverding, C.H., 1976, "Transonic Flows in Axial Turbomachinery", VKI Lecture Series 84

Spalart, P. R., Allmaras, S. R., 1994, "A One Equation Turbulence Model for Aerodynamic Flows", La Recherche Aerospatiale, No.1, pp 5-21

Stauter, R.C., Dring, R.P., Carta, F.O., 1991, "Temporally and Spatially Resolved Flow in a Two-Stage Axial Compressor: Par 1 – Experiment", ASME Journal of Turbomachinery, Vol. 113, pp. 219-226

Zaccaria, M.A., Lakshminarayana, B., 1995, "Investigation of Three-Dimensional Turbine Flow Field at the Exit of the Nozzle", J. of Propulsion and Power, Vol. 11, pp. 55

Zaccaria, M.A., Lakshminarayana, B., 1997, "Unsteady Flow Field Due to Nozzle Wake Interaction With the Rotor in an Axial Flow Turbine: Part II – Rotor Exit Flow Field", ASME Journal of Turbomachinery, Vol. 119, pp. 214-224

Zunino, P., Ubaldi, M., Campora, U., Ghiglione, A., 1997, "An Experimental Investigation of the Flow in the Trailing Edge Region of a Turbine Cascade", Proceedings of the 2nd European Conference on "Turbomachinery – Fluid Dynamics and Thermodynamics", Antwerpen